Energy & Buildings 289 (2023) 113066

Contents lists available at ScienceDirect

Energy & Buildings

journal homepage: www.elsevier.com/locate/enb

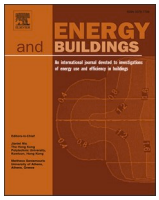

Assessment of basic control strategies through dynamic simulations: A CO2-based chiller under extreme off-design conditions

Enrico Sisti [a,*], Antonio Rossetti [c], Silvia Minetto [c], Sergio Marinetti [c], Giacomo Tosato [d], Alessandro Beghi [a], Mirco Rampazzo [a,b]

[a] University of Padova, Department of Information Engineering (DEI), Padova, Italy
[b] University of Padova, Department of Industrial Engineering (DII), Padova, Italy
[c] National Research Council (CNR), Construction Technologies Institute (ITC), Padova, Italy
[d] Enex srl, Paese, Province of Treviso, Italy

ARTICLE INFO

Keywords:
Carbon dioxide
Transcritical cycle
Heat pump
Chiller
Modelling
Simulation

ABSTRACT

Modelling and simulation tools offer peerless possibilities to dominate the increasing complexity of industrial applications, accelerating innovation cycles by quickly exploring and exploiting new efficient, reliable, and green possible solutions. In this paper, a dynamic model of a chiller system is developed through a mixed causal and acausal modelling approach. The chiller system uses carbon dioxide as a refrigerant and satisfies the cooling needs of high energy-demanding buildings. The model is validated against experimental data under various operating conditions and can be used to investigate the performances of different control logics under a wide partialization spectrum ranging from around 15% to 100% of the design cooling power of the system. Three simple control strategies, combining rule-based control and PID control, are presented and compared through both steady load simulations and daily characterizations. Simulation results point out opportunities that arise from the integration of the presented model in Computer-aided Control System Design (CACSD) software tools.

1. Introduction

In recent years, regulations, as F-gas regulation in Europe, and international protocols, such as the Kigali Amendment to the Montreal Protocol, have pushed research and industry towards the use of CO2 (R744) as a refrigerant also in heat pumps for comfort heating and cooling. Due to its negligible Global Warning Potential (1 or 0), while being non-toxic, non-flammable and future-proof safe for human beings and environment, the use of carbon dioxide as a refrigerant may prove to be of paramount importance in meeting the growing demand for energy-efficient and environmentally sustainable refrigeration solutions in the long term. Also, Heating, Ventilation, Air Conditioning, and Refrigeration (HVAC&R) systems account for a great amount of energy consumption, and their inefficient operation translates into poor performance and increasing costs, global emissions, and the environmental footprint of human activities [1]. It is worth mentioning that energy efficiency is at the heart of European Green Deal's mid (i.e. 2030) and long-term (i.e. 2050) goals for smart, sustainable and inclusive growth and of the transition to a resource efficient economy [2]. In this context, developments in the design and optimisation of heat pump operation are essential to reduce the carbon footprint of heating and cooling applications.

Nowadays, improving energy efficiency involves the use of advanced control systems [3], which offer the distinctive opportunity to remarkably improve both efficiency and effectiveness by mainly acting on software components. However, the presence of nonlinear behaviours, together with non-stationary system operating conditions, complex patterns of user demand, coupling effects, and much more, make the control of HVAC&R systems a challenging task [4]. Besides, the COVID-19 pandemic has posed new challenges to the design and the management of these systems. In recent years, researchers have analysed the effect of the pandemic both on the utilization of HVAC&R systems when draconian measures were in place in several countries [5,6], and on their future operation due to new policies and guidelines [7,8] formulated by various organizations around the world to control and mitigate indoor infection risks. In [9,10], the authors focused on the design and operational variations suggested by different guidelines and delved into their impacts on energy consumption compared with pre-pandemic situation. Alongside design solutions (e.g. HEPA filters, UVGI systems, heat recovery equipment, etc.), all guidelines highlight the importance of increasing both room ventilation rates and outdoor air ratios, and of

* Corresponding author.
E-mail address: enrico.sisti@phd.unipd.it (E. Sisti).

https://doi.org/10.1016/j.enbuild.2023.113066
Received 16 December 2022; Received in revised form 24 March 2023; Accepted 6 April 2023
Available online 7 April 2023

Nomenclature

ρ	density (kg m^{-3})
p	pressure (bar)
T	temperature (°C)
h	specific enthalpy (J $kg^{-1}K^{-1}$)
g	gravitational acceleration (m s^{-2})
z	height (m)
$\dot{m}$	mass flow rate (kg/s)
FS	full scale
Δ	difference operator
$\dot{Q}$	heat transfer rate (W)
P	Power (W)
COP	Coefficient of Performance (-)
DC	compressor duty cycle (-)
PR	pressure ratio (-)
S	control strategy
n	compressor rotational speed [rpm]

Subscripts

amb	ambient conditions
BPV	back-pressure valve
FE	flooded evaporator
LPR	low-pressure receiver
LP	low pressure
in	inlet
A	tank-FE water loop
1–8	refrigerant gauge ports (as in Fig. 1)
load,0	experimental thermal load
0	reference control logic
T	temperature controlled
liq	refrigerant liquid condition
C	compressor
GC	gas-cooler
HP	high pressure
out	outlet
B	tank-building water loop (Fig. 1)
load	thermal load
2x, 3x	multiplication factors
P	pressure controlled

extending the running time of HVAC&R systems. If on the one hand higher ventilation rates and outdoor air ratio tend to raise the thermal loads (also depending on local weather), on the other extra running hours can lead these systems to operate under low part load ratios, which may negatively affect their energy efficiency. In either case, developing effective control strategies to efficiently manage the functioning of these systems even under off-design operating conditions is a key task to minimise their energy consumption.

In this scenario, some research efforts have been made to address the need for a trade-off between thermal comfort, indoor air quality, and energy consumption of HVAC&R systems. In [11], a comprehensive dynamic model of a medium office building and a variable-air-volume (VAV) supply system, equipped with a virus transmission model and different models for air filtration, was used to compare different strategies designed to increase indoor air quality and assess the energy use. A quasi-steady state model of a high-efficiency air handling unit (HEAHU) was considered in [12] to investigate the integration of a heat pump into traditional air handling units (AHUs) or as stand-alone, combined with a heat recuperator, for energy recovery purposes. The results underlined the effectiveness of this solution in alleviating the increase of energy consumption due to the higher ventilation rates needed to reduce the infection risk in school environments. Risbeck et al. [13] adopted physics-based balances for an AHU system, and phenomenological models for the control system, to predict airflows and the energy consumption. This model was then coupled to the dynamic model of a building, which embedded both thermal dynamics of the spaces and the dynamic model of airborne disease transmission, to perform multi-objective optimization and evaluate the trade-off between infection risk and energy consumption. The proposed optimization framework aimed to find Pareto-optimal values over a set of design variables and operational setpoints. In [14], the authors developed a model predictive control (MPC) algorithm based on machine learning models for the prediction of building occupancy and a simple thermal dynamic model of the space, whose parameters (e.g. HVAC system efficiency) were calibrated against real data. The occupancy prediction model was used to compute the minimum outdoor air needed to reduce aerosol transmission, while the building thermal model provided the cooling load. The aim of the MPC control system was to minimise the energy consumption while ensuring thermal comfort and indoor air quality, by determining the optimal values of the supplied air flow, temperature, and outdoor air ratio.

Although the literature review highlighted growing attention on energy consumption and control topics, current studies lack detailed and consistent analysis of HVAC&R systems operation under off-design conditions, which can significantly impact the performance of both the systems and their control systems. The nonlinear behaviours of heat pumps and chiller, coupling effects and the multidisciplinary approach required to discuss both the system and its control represent the main challenges to the development of efficient and effective system management strategies under technological constraints. In this scenario, modelling, and simulation tools offer great opportunities to dominate the growing complexity of technologies, thereby providing inestimable support for the design and the analysis of the refrigerating system. In addition, simulation environments accelerate innovation cycles by quickly exploring new solutions. Also, when compared with real-world experiments, the use of these software tools is generally cheaper, faster, and more flexible than in-house tests as they easily allow to configure the environment parameters to reproduce the operational application field of the final product [3]. Therefore, once defined the boundaries (e.g. thermal load and outdoor temperature profiles), validated models can reliably be used to forecast the performance of the system, especially under conditions that are difficult to replicate in experimental tests. Besides, as this kind of systems is characterised by various subsystem dynamic interactions, numerical models can represent valuable tools to test different control logics for operation optimisation and energy consumption minimisation in a better integrated Co-Design approach [15-17]. Indeed, synthetic environments play a crucial role when it comes to deploy co-simulation methods to design the entire system and reach optimal solutions, while considering all the multidisciplinary aspects of the system.

Many different control techniques can be found in literature, both classical control architectures and advanced control algorithms [18]. Classical control architectures are the most intuitive and the easiest to be implemented and usually include rule-based control and standard regulators (PID). As drawbacks, rule-based control can lead to noticeable lacks in minimizing energy consumption, while an improper choice of the gains in the PID controller could produce stability problems of the systems [19]. Moreover, their performance is subject to degradation as result of large variations of the operating conditions or in case of time delays due to high time constant of the system [20]. In HVAC&R applications, the main control objective is to satisfy heating and cooling demands while guaranteeing overall stability of the system. Cooling

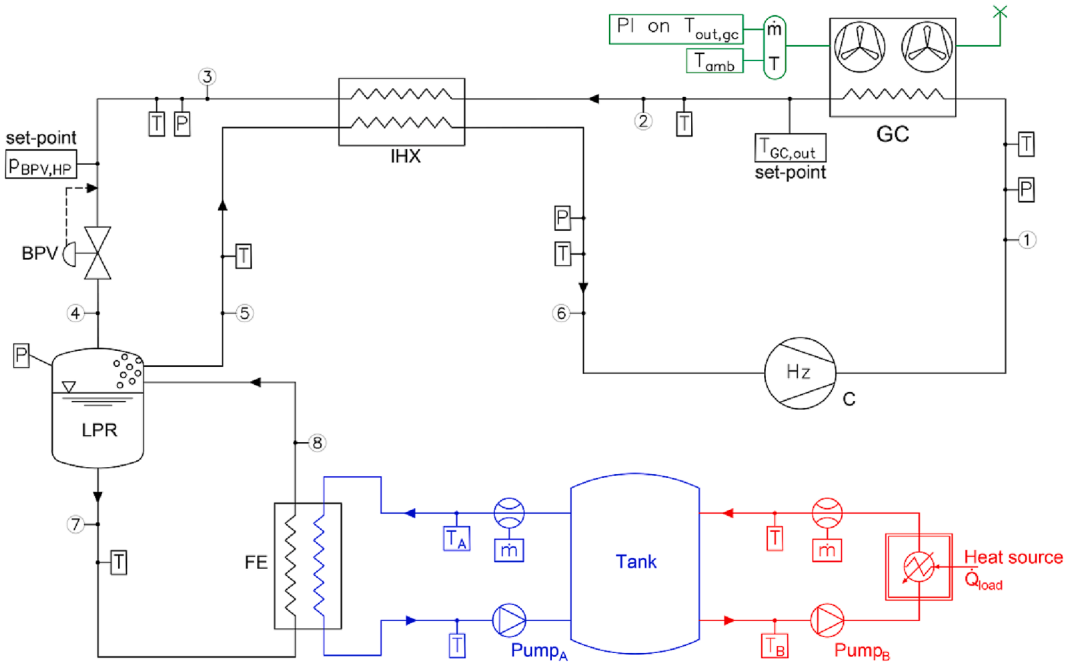

Fig. 1. Operating scheme of the transcritical heat pump represented in chiller configuration.

power in chillers and refrigerating systems is traditionally intended to be controlled through compressor ON/OFF cycling and the outlet temperature of the evaporator secondary fluid or the evaporating pressure/temperature of the refrigerant, using the compressor speed as manipulated variable [21,22].

On the other hand, advance control systems can overcome the previously mentioned limitations combining techniques, such as optimal, adaptive, and predictive control, and exploiting the technological advances in data storage, computing, and communication devices [18,23,24]. In this scenario, modelling and simulation tools offer a significant contribution to accelerate the design and the development of control algorithms to embed quite complex decision-making capabilities in HVAC&R systems. Indeed, models mimicking relevant HVAC&R system dynamics can be integrated in Computer-aided Control System Design (CACSD) software tools to generate synthetic data and to design and assess different control strategies.

In this paper, we propose a dynamic model of a refrigerating system to compare different control strategies under mild and heavy partialized loads. The aim of this work is to contribute to bridge the gap in the literature with a consistent analysis of the performance of the chiller operating under off-design conditions, thereby gaining useful insight about the system behaviour from a control design perspective. Moreover, the proposed model can serve as a valuable tool for the design and optimization of refrigeration systems in various applications. The remainder of the paper is organised as follows. Section 2 presents the reference system, its operating scheme, processes, and experimental apparatus. Section 3 summarises the mathematical model of the refrigerating system, with specific emphasis on the newly developed model of the natural circulation evaporator, and the overall validation of the dynamic model in transient operation. Three different control strategies are described in Section 4 and their performances are compared and discussed in the results section (Section 5). Lastly, Section 6 provides concluding remarks and further possible developments related to the findings presented in this paper.

2. System configuration and experimental apparatus

The configuration considered in this manuscript derives from an original design of a chiller with heat recovery presented in [25], where two evaporators are used, being the refrigerant ejector-driven in the first one and naturally circulated in the second one. The present paper focus mainly on the natural circulation evaporator, which is considered as represented in Fig. 1.

The system is powered by an inverter controlled semi-hermetic compressor (C) whose rotational speed is regulated on the evaporation pressure. Compressor suction line is connected to the low-pressure receiver (LPR) by means of an internal heat exchanger (IHX). Then, the refrigerant flows in a finned coil gas-cooler (GC) where rejects heat to an external air stream. The rotational speed of the axial fans installed at the gas-cooler outlet is modulated by a PI controller designed to maintain the refrigerant outlet temperature at the prescribed set point $T_{GC,out}^{set-point}$. Then, the refrigerant is further cooled by passing through the high-pressure side of the internal heat exchanger and it is subsequently expanded to the evaporation pressure by a back-pressure valve (BPV), which is regulated by a PI controller to maintain its inlet high-pressure set-point $p_{BPV,HP}^{set-point}$.

After the expansion, the two-phase mixture enters the low-pressure receiver (LPR), that acts as a separator of the liquid and vapour phases. The lower and the upper part of the receiver are connected to the refrigerant ports of a brazed plate heat exchanger (FE). The other ports are arranged to realize a counter flow heat exchange with the secondary fluid (water). Refrigerant is driven through the evaporator by means of buoyancy driven natural convection. The force driving the refrigerant through the evaporator depends on the density difference between liquid and gaseous phase at the evaporator input and output. In the water circuit, the flooded evaporator is fed by a recirculating pump ($Pump_A$) connected to an insulated water tank. Then, a second recirculating pump ($Pump_B$) supplies the air conditioning system of the hotel.

A real system following the scheme of Fig. 1 was installed in a hotel located in a touristic area in North Italy and monitored under actual operating conditions in the period from June to September 2020. In the experimental apparatus, sensors and transducers are installed according to Fig. 1. Experimental data was collected using a three-phase network analyser and current transformer (accuracy 0.5% FS, with FS equal to 130 kW), eleven T-type thermocouples (accuracy ±0.2 K), four pressure transducers (accuracy of ±0.24 bar), and two electromagnetic flowmeters for the water streams (accuracy of 1 % on the read value with

Table 1
Dimensions of the heat pump main components.

Compressor (C)	Reciprocating, semi-hermetic, single stage compressor. Displacement volume 180.69 cm^3 Nominal speed 1450 rpm@50 Hz
Gas-cooler (GC)	Finned coil heat exchanger. Heat transfer area: External area 491.2 m^2 Internal area 64.6 m^2
Internal heat exchanger (IHX)	Counter flow, tube-in-tube type heat exchanger. Heat transfer area: Low pressure side 0.108 m^2 High pressure side 0.125 m^2
Back-pressure valve (BPV)	Electrically operated step motor valve. Maximum opening diameter 5.8 mm
Low pressure receiver (LPR)	Horizontally oriented cylindrical carbon steel receiver. Internal volume 0.167 m^3 Internal diameter 406 mm
Flooded evaporator (FE)	Counter flow, single pass brazed plate heat exchanger. Heat transfer area of 7.62 m^2

velocity between 0.4 and 10 ms^{-1}).

The control strategy of the heat pump involves a sequence of actions based on the monitored temperature T_B of the water supplied to the building by $Pump_B$ and the evaporation pressure in the receiver. Firstly, the water pump $Pump_A$ is switched on when the supply water temperature is higher than a certain threshold. Later, once a predefined receiver pressure value is reached, gas-cooler fans are activated and then the compressor is started. Finally, the refrigeration system and the water pump $Pump_A$ are turned off when the receiver pressure and the supply water temperature fall below their corresponding set-point values, while $Pump_B$ is maintained in operation.

Table 1 summarises the geometric dimensions of the system main components.

3. Numerical model

Obtaining a dynamic model that ensures a good balance between model simplicity and accuracy is a non-trivial task. Indeed, even if the governing physical laws are known, the formulation of specific relationships is usually a laborious task and, in many cases, it requires knowledge of the values of parameters that are difficult to derive. To develop a simple but enough accurate dynamic model, the following simplifying assumptions were made. According to [26], the dynamics of mass flow devices (i.e. compressor and back-pressure valve) are generally one order of magnitude faster than energy flow devices (i.e. heat exchangers and low-pressure receiver). Therefore, since we are interested in studying the interactions of slow dynamic phenomena, the compressor and the back-pressure valve can be considered static components and modelled by resorting to steady-state empirical correlations. Different approaches were instead used to modelling the dynamic components: the low-pressure receiver was conceived as an adiabatic volume with homogeneous pressure and specific enthalpy; the heat exchangers were modelled as an approximation to a simple straight tube in perfect counter flow configuration, then discretised into smaller volumes with a lumped parameters approach. The overall performances of each heat exchanger were validated at nominal conditions against manufacturer's data. The complete description of these sub-models is beyond the scope of this article. For the complete formulation and more details see [25,27].

A mixed causal and acausal modelling approach [28] was considered and the software Simcenter Amesim v2021.2 was used. The main components of the system (i.e. compressor, gas-cooler, internal heat exchanger, back-pressure valve, low-pressure receiver, flooded evaporator, and control systems) were modelled by exploiting the libraries of the software (i.e. acausal approach where models essentially are expressed in terms of undirected equations), which provide basic elements designed to simulate the transient behaviour of internal and external flows, i.e. refrigerant, water and ambient air. Each component was represented by a sub-model, obtained by coupling basic elements, and then the complete heat pump model was developed by connecting the sub-models in the same way as shown in the previously described operating scheme. Conversely, the libraries lack sub-models that reproduce the driving force due to the difference between the density of liquid and gaseous phases at the inlet and the outlet of the flooded evaporator. Therefore, the characterisation of the natural circulation of the refrigerant through the heat exchanger required a causal approach (where the outputs are explicitly expressed in terms of the inputs, i.e. the

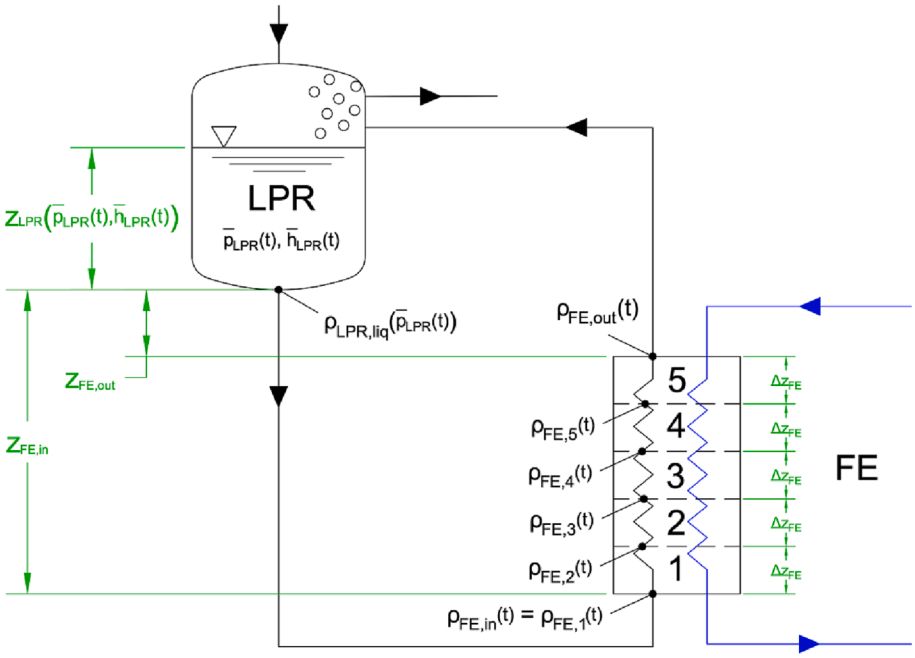

Fig. 2. Schematic of the discretised natural circulation flooded evaporator coupled to the low-pressure receiver and the water circuit.

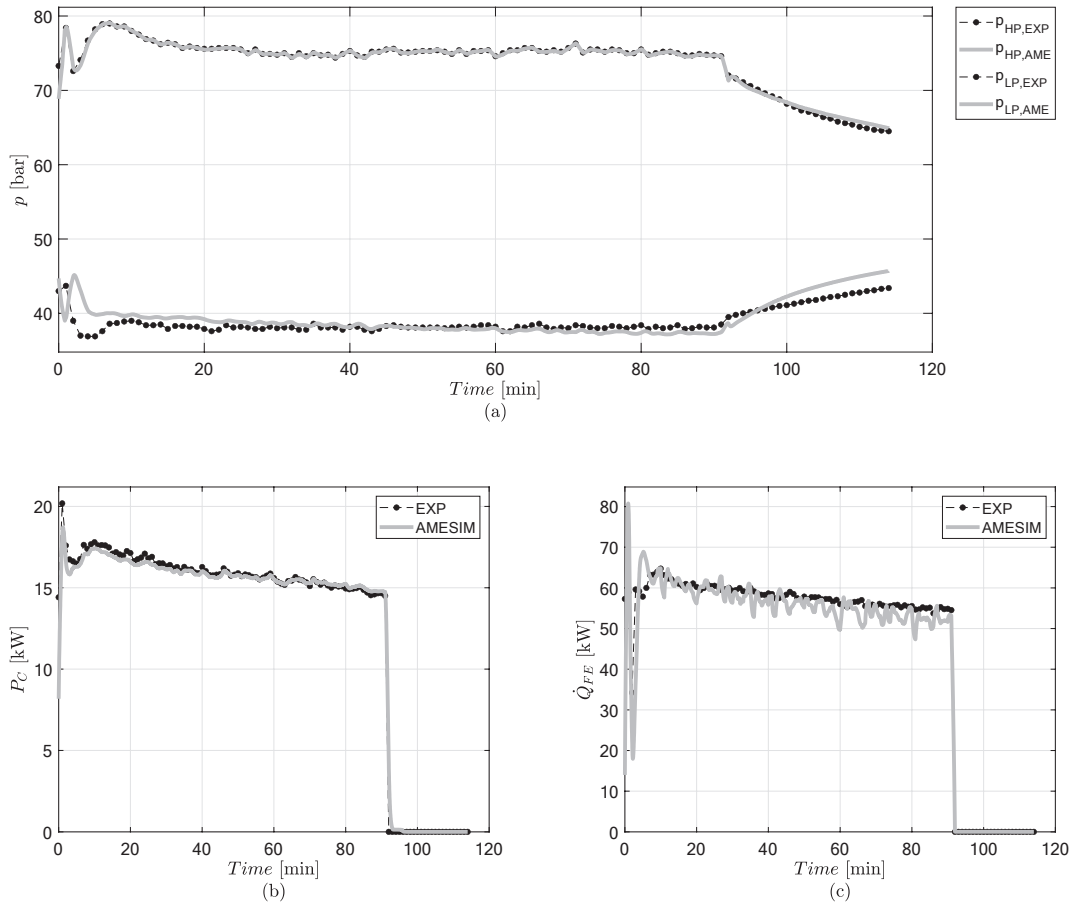

Fig. 3. Comparison between observed and predicted (a) compressor discharge and suction pressures, (b) compressor power consumption, and (c) cooling capacity, of the second on–off cycle of the VI operating condition.

direction of information flow is manifest), as illustrated in the following paragraph.

3.1. Dynamic numerical model

The detailed description of the numerical model of the system is presented in [25], apart from the natural circulation evaporator (FE, Fig. 1), whose model is described below.

The density gradient, determined by the heat transferred in the heat exchanger, induces the natural circulation of the refrigerant in the flooded evaporator. Due to the lack of a proper sub-model in the software libraries, this phenomenon was modelled considering the inlet specific enthalpy and the outlet pressure of the evaporator respectively equal to the specific enthalpy of the saturated liquid and to the average refrigerant pressure $\overline{p_{LPR}}$ in the receiver. According to Eq. (1), the inlet pressure was determined from $\overline{p_{LPR}}$ by adding the pressure increase Δp_{FE} corresponding to the difference between the liquid static head and the two-phase static head, which varies along the heat exchanger. Fig. 2 depicts the discretised flooded evaporator coupled to the low-pressure receiver. The height of the liquid-vapour interface z_{LPR} and the saturated liquid density $\rho_{LPR,liq}$ depend on the refrigerant state in the receiver, while the densities in the flooded evaporator $\rho_{FE,k}$, with $k \in [1,5]$, are also function of the heat exchanged and the pressure losses. In addition, the heights of the inlet $z_{FE,i}$ and the outlet $z_{FE,o}$ of the evaporator were drawn from the geometric characteristics of the refrigerating system. Lastly, as the heat exchanger is vertically oriented, the height increment Δz_{FE} was set equal to the length of each discretised element.

$$\Delta p_{FE} = g\left[\rho_{LPR,liq}\left(z_{LPR}+z_{FE,i}\right) - \rho_{FE,out}\left(z_{LPR}+z_{FE,out}\right) - \Delta z_{FE}\sum_{k=1}^{5}\rho_{FE,k}\right]. \quad (1)$$

The thermodynamic properties of carbon dioxide were evaluated with the Modified Benedict Webb Rubin (MBWR) formulation, which considers the pressure as a function of the fluid density and temperature, while the presence of oil in the refrigerant flow and the effect of gravity were neglected. Also, the assumption of pure water was made, and Bode's formulation was used to calculate its thermodynamic properties. Moreover, the air was considered as a mixture composed by a combination of pure fluids weighted by their concentrations.

The parameters of the numerical model are the geometric dimensions of the main components (see Table 1) and the refrigerant charge (here considered equal to 160 kg), while the inputs are the water temperature and mass flow rate at the evaporator inlet, the external ambient temperature to set the air inlet conditions at the finned coil gas-cooler, and the thermal load $\dot{Q}_{load}$ on the water loop serving the building fan coil. The model provides as outputs the physical state of each of the 160 state variables, which can be used to compute the heat flow rates in the heat exchangers and the compressor power consumption.

3.2. Dynamic validation

The validation of the numerical model was performed in transient operation. The thermal performances of the model in chiller configuration were compared to experimental data collected from a real system, which serves a hotel located in a touristic area in North Italy, under

Table 2
Comparison between experimental data and simulation results in ON state conditions of the chiller.

		Selected operating conditions								
		I	II	III	IV	V	VI	VII	VIII	IX
p_1	AME [bar]	61.0	64.3	66.6	69.5	73.0	75.4	81.0	82.0	84.4
	MPE [%]	**0.0**	**0.0**	**0.1**	**0.2**	**0.1**	**−0.1**	**0.1**	**0.0**	**−0.1**
p_6	AME [bar]	39.5	38.8	39.1	38.5	38.8	38.5	38.3	38.7	38.5
	MPE [%]	**3.0**	**2.4**	**2.4**	**0.4**	**1.5**	**0.6**	**−0.9**	**−0.2**	**−0.3**
P_C	AME [kW]	10.0	12.0	12.8	14.4	15.6	15.9	18.0	18.1	19.2
	MPE [%]	**−5.7**	**−4.2**	**−3.0**	**−1.8**	**−2.2**	**−1.0**	**−0.1**	**−0.4**	**−0.3**
$\dot{Q}_{FE}$	AME [kW]	58.4	61.7	59.7	64.9	63.8	57.8	62.9	61.9	62.3
	MPE [%]	**9.9**	**11.6**	**2.1**	**6.4**	**6.1**	**0.1**	**8.1**	**8.9**	**5.9**

actual operating conditions in the period from June to September 2020. The experimental data were collected within the MultiPACK Project, funded by the European Union's Horizon 2020, and published in an open database [29]. Nine different operating conditions, which depend on the ambient conditions, were selected to cover the range of possible case studies in terms of high-pressure values of the system (approximately 60 bar $\leq p_1 \leq$ 90 bar). The respective data sets included two consecutive on-off cycles of the refrigerating unit, corresponding to time interval values between 3 and 5:30 h. The first cycle made it possible to reduce the effect of model initialisation conditions on simulation results, while the second cycle was subsequently exploited to validate the model.

The experimental data were used to set the boundary condition of the model and to define the compressor starts and actual speed. During the ON state, the refrigerant high pressure p_3 and the gas-cooler outlet temperature T_2 were controlled to match the experimental trends, by acting on the BPV and on the gas cooler air mass flow rate. Therefore, the validation was carried out comparing experimental and simulated trends of evaporation pressures p_6, compressor power consumptions P_C, and cooling capacities $\dot{Q}_{FE}$.

Fig. 3 depicts the validation variables for one of the validation sets (the on–off initialization cycle is not reported).

Table 2 summarises the mean values of numerical results and mean percentage errors (MPE) between the simulated and experimental values for ON state conditions of all selected case studies. Both simulated and experimental cooling capacity were calculated according to Eq. (2).

$$\dot{Q}_{FE} = \dot{m}_C(h_6 - h_2). \tag{2}$$

It is worth mentioning that temperature sensors are installed on the external side of the pipes, thus providing a low pass filtering effect of the measured signals. This may explain the less noisy performance of experimental cooling capacity compared to the numerical one, as well as the lack of damping factors in the model components with respect to the real system.

Numerical model demonstrated a reasonable accuracy, with maximum and mean errors on the cooling power of 11.6% and 6.6 % respectively, considering that the aim of the model is to test and compare different control strategies in a consistent way.

4. Control strategies

The simulation environment can be deployed to generate synthetic data related to some fundamental aspects of the thermal behaviour of the refrigerating system, as well as to design and test different control strategies to efficiently manage the system.

The validated numerical model was used to simulate the operation of the refrigerating unit in chiller configuration coupled with a stratified water storage tank, as illustrated in Fig. 1. The aim was to highlight the model usefulness to discuss different control strategies and to promote the development of innovative ones. In the following, we compare two different control logics for the compressor speed, against a constant speed on/off approach, used as a baseline.

All the three considered controls share the same logic to define the state of the recirculation pump ($Pump_A$) and the compressor on/off cycles. The water pump $Pump_A$, is switched on when the temperature of the water supplied to the building T_B was higher than 12 °C and it is turned off with T_B lower than 5.5 °C. The same signal used to switch the state of the pump $Pump_A$ is used to switch on or off the compressor. The limit of 12 °C is, for the considered case, the highest allowable temperature T_B according to installed AC terminals and the system nominal power. The three controls use different inputs and approaches to set compressor rotational speed during the ON period.

In the baseline control system, the compressor rotates at constant nominal speed (corresponding to 50 Hz frequency). This is referenced as S_0 control strategy, as no active control is used to adjust the compressor speed. In this case the evaporation pressure is not directly controlled and arise naturally to equilibrate the flooded evaporator heat exchange and the compressor capacity.

The second logic uses the evaporation pressure p_6 to modify the compressor speed, and thus the cooling capacity, by linearly varying the compressor frequency between 60 Hz, for $p_6 \geq 47$ bar (i.e. 11.74 °C), and 30 Hz, for $p_6 \leq 35$ bar (i.e. 0.16 °C). This pressure driven control of the cooling capacity is inspired to the actual control of the reference unit and it follows the recommendation reported by ASERCOM [22].

Instead of the evaporation pressure, the third control system uses the water temperature at the delivery point T_B as control variable. While the first two are purely rule-based control logics, in this case a bounded PID controller is included to manage the compressor speed. For $T_B \leq 12$ °C the compressor speed is maintained at 30 Hz, and the compressor on-off cycles are defined by the hysteresis cycles between 5.5 and 12 °C of T_B as in the S_0 control. When the temperature T_B reaches the maximum allowed value of 12 °C, the PID controller increase the compressor frequency up to 60 Hz to contrast any further increase in T_B. A proper tuning of the PID constants (especially the derivative part) was carried out to prevent T_B to cross the limit of 12 °C. This temperature-based control was modelled according to ASHRAE [21].

As the control logics S_p and S_T imply the use of an inverter, to have a fair comparison of the actual systems energy consumption with S_0, a conversion efficiency of 0.95 for the inverter was accounted in the variable speed logics.

The inputs to the numerical model were the temperature of the air entering the gas-cooler assumed equal to the ambient temperature T_{amb}, the constant value of the water mass flow rate pumped by $Pump_A$ and flowing through the flooded evaporator, the water mass flow rate supplied by $Pump_B$, and the thermal load $\dot{Q}_{load}$. All the boundary conditions and set-points, both single values, in case of steady-state simulations, and profiles, in case of dynamic simulations, were taken from a

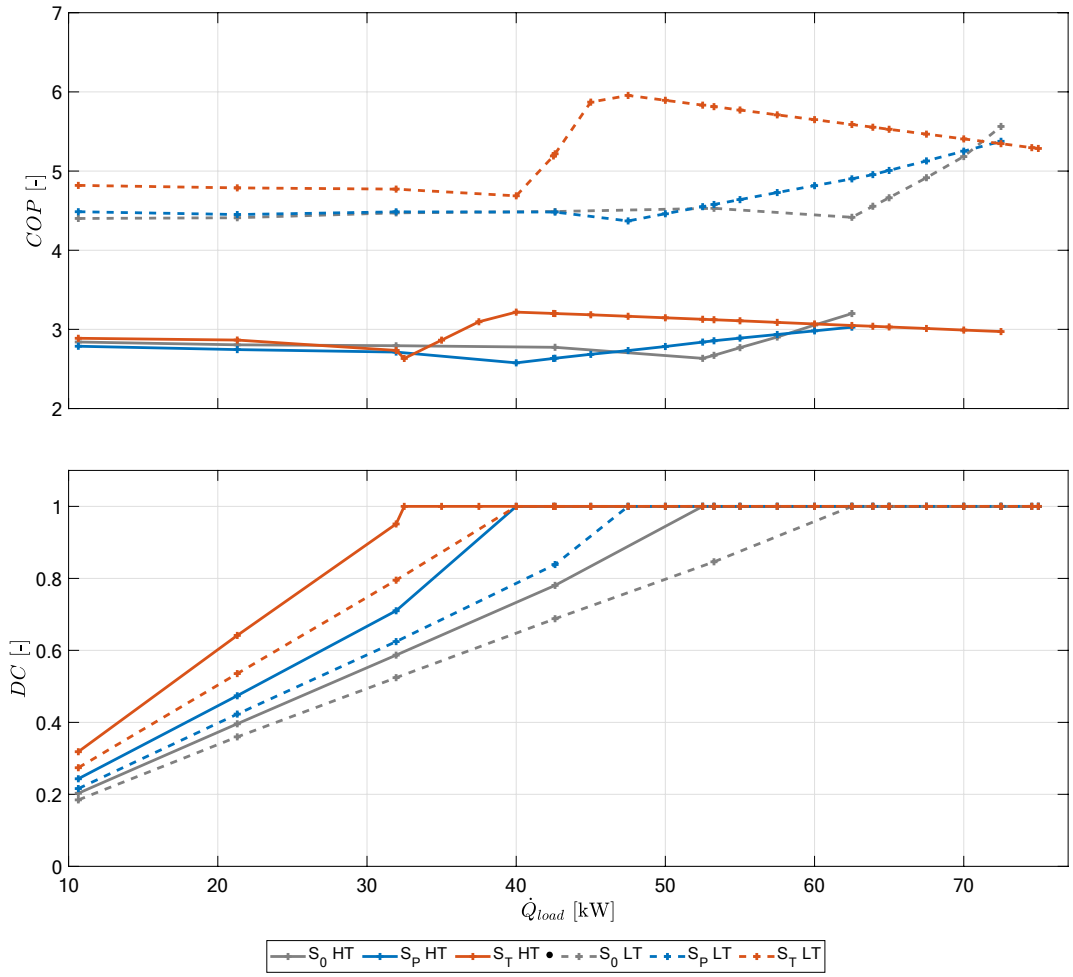

Fig. 4. Simulations results under steady-boundary conditions - Coefficient of Performance (COP) and Compressor Duty Cycle (DC).

representative day of summer season (31st July 2020) extracted from experimental data.

During operation, the refrigerant temperature $T_{GC,\,out}^{set-point}$ at the gas-cooler output and the refrigerant high-pressure $p_{BPV,HP}^{set-point}$ at the inlet of the back-pressure valve were modulated by PI controllers to ensure the corresponding set-point values, which depend on the ambient temperature T_{amb}. For the purposes of this work, the energy consumptions related to gas-cooler fans and water pumps (i.e. $Pump_A$ and $Pump_B$) were neglected.

5. Results

In the section that follows, we report upon the performances of the refrigerating unit simulated in chiller configuration coupled with a water storage tank and controlled by the control logics described above.

5.1. Chiller characterization under steady loads and boundary conditions

Firstly, the control strategies were tested under several steady boundary conditions and disturbances, taking as input different values of the thermal load $\dot{Q}_{load}$ in the working range of the chiller from 10.7 kW to 74.6 kW. The system was characterized for two different ambient temperatures T_{amb}, corresponding to a mild (20.7 °C, LT) and hot condition (30.4 °C, HT).

While for high loads the chiller and the hydronic loop can find a stable equilibrium, at partial load the system reaches a periodic response with a stable Duty Cycle (DC), where the chiller stores the cooling power in the water tank and then stops until the increase in the tank temperature causes the following ON period. Fig. 4 shows the Coefficient of Performance COP and the compressor duty cycle for each control strategy and each temperature level as a function of $\dot{Q}_{load}$. Although the whole range was studied for each of three control logics, the data reported in Fig. 4 are limited to the operation points that satisfy the maximum water temperature condition $T_B \leq 12$ °C.

It is worth noting that when DC was less than one, the COPs were calculated as the ratio between the total cooling energy, provided by the flooded evaporator, and the total compressor energy consumption during the last ON state condition of the refrigerating system. Conversely, when the system operated continuously (i.e. DC equal to one), the COP corresponded to the ratio between the cooling capacity and compressor power consumption measured once the system reached a steady equilibrium.

As previously described, the water supplied to the building T_B varies in the same range within each ON-OFF cycle. The temperature T_B is coupled to the temperature of the water supplied to the flooded evaporator T_A through the dynamic of the water tank, and this means that T_A, and consequently the evaporation pressure, remains in similar ranges even though the thermal load changes significantly. Besides, the high pressure is controlled by the back-pressure valve on the ambient temperature. Therefore, the COP of the system depends mainly on the ambient temperature of the air to which the heat is released from the gas-cooler, and secondary on the compressor frequency determined by each control system, while it is less affected by the thermal load, which, on the other hand, certainly has an impact on the DC. For these reasons, little differences can be observed between the performances of the

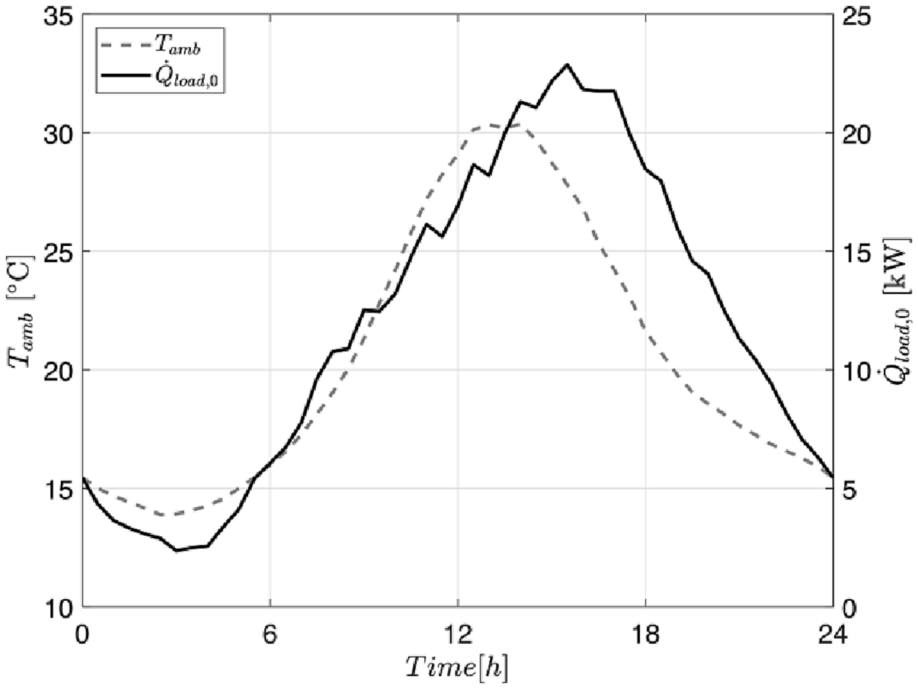

Fig. 5. Experimental ambient temperature T_{amb} and thermal load $\dot{Q}_{load,0}$ profiles.

control logics in terms of COPs when the corresponding DC is less than one for the same temperature level.

Major differences can be highlighted when continuous operation is reached, i.e. when DC is equal to one. In this case, the temperature T_A reached constant values depending on the action of each control system. Higher values of T_A led to higher evaporation pressures and lower pressure ratios. As a result, the control logic that provided higher evaporation pressures, for the same thermal load and ambient

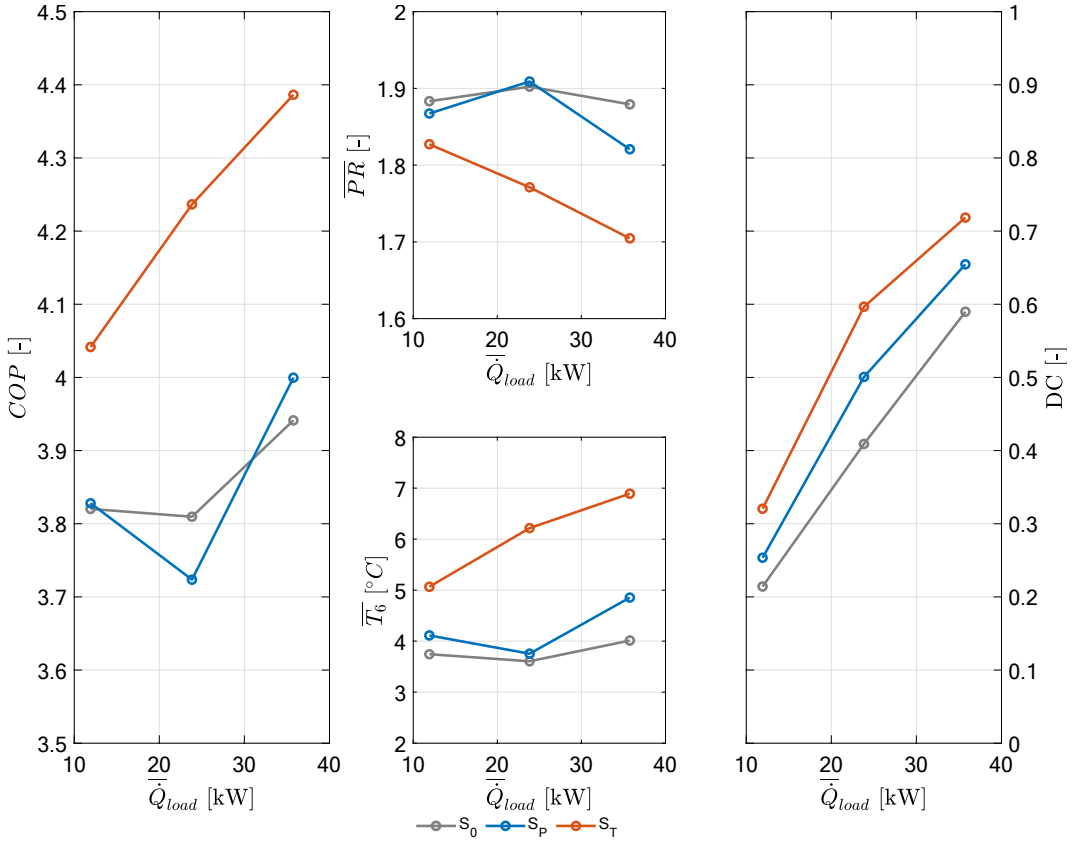

Fig. 6. Overall performances of the control strategies for all the tested thermal loads profiles: mean value of the Coefficient of performance (COP), average Pressure Ratio (PR), average evaporation temperature T_6, and overall Compressor Duty Cycle (DC), versus thermal load average value $\overline{\dot{Q}}_{load}$.

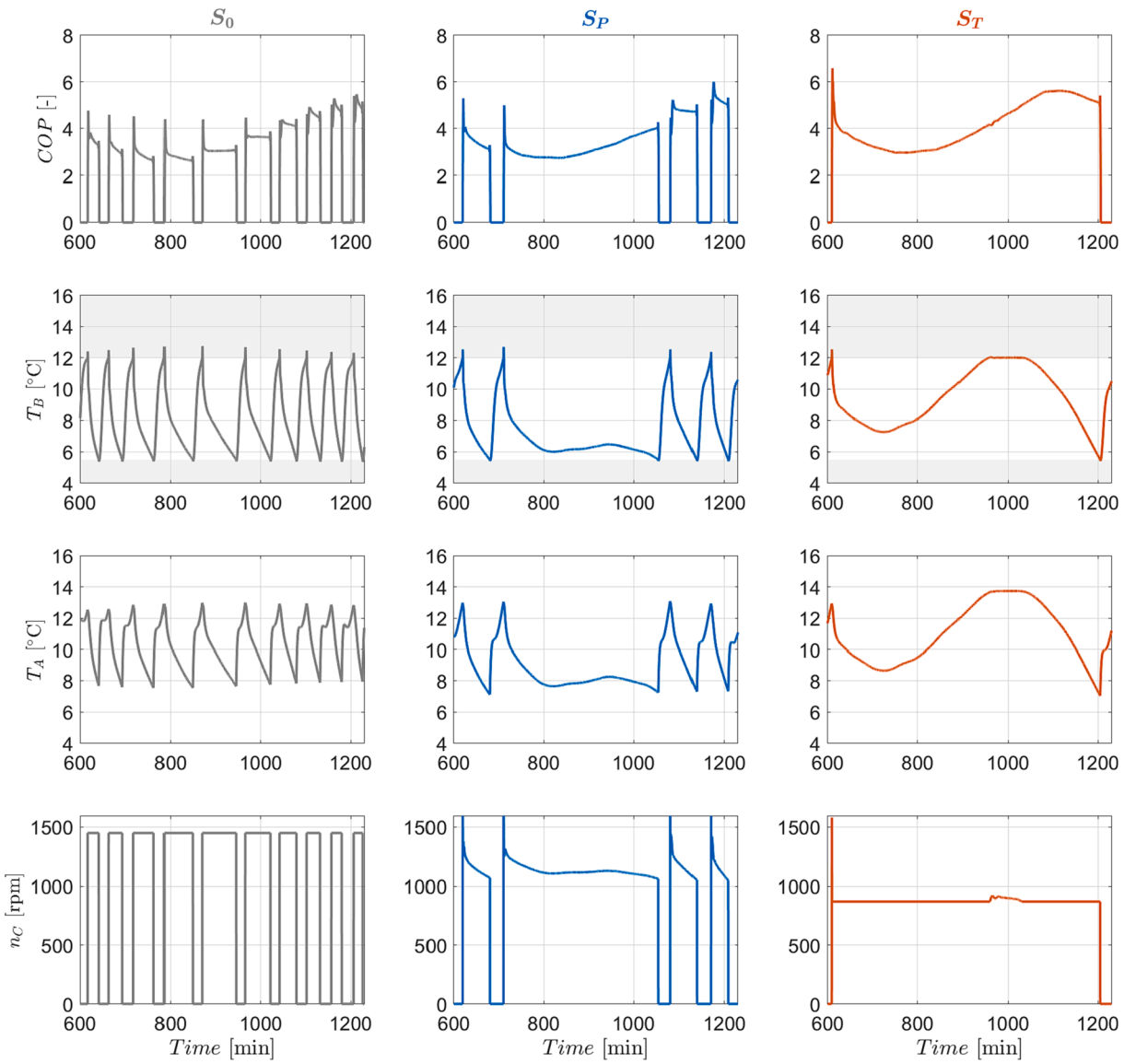

Fig. 7. Comparison between simulation results for the thermal load profile $\dot{Q}_{2xload,0}$: coefficient of performance (COP), temperature T_B of the chilled water supplied to the hotel, temperature T_A of the water supplied to the flooded evaporator, and compressor rotational speed n_C (nominal speed equal to 1450 rpm@50 Hz).

temperature, gained considerable advantages in terms of energy efficiency of the system.

After reaching DC equal to one, increases in the values of the COP can be noticed for all the considered control systems. This can be explained by the fact that the strategies S_0 and S_T were designed to keep constant the initial compressor frequency (i.e. 50 Hz and 30 Hz respectively) for T_B within the range 5.5–12 °C, and a proportional increase in the compressor rotational speed was considered for S_P in the same range. So, for temperature T_B lower than 12 °C, increasing values of the thermal loads determined higher evaporation pressures, thus positively affecting the performances of the system. Beside that, S_T showed decreasing values of the COP once the PID controller intervened increasing the compressor frequency to maintain the temperature T_B at 12 °C. In this situation, higher thermal loads led to higher compressor frequencies, while the evaporation pressures remained nearly constant, thus raising the energy consumptions of the compressor.

The strategy S_T overtook the other logics in almost the whole range of the explored thermal loads, but especially for medium/high thermal loads. This is in accordance with its design goal which was to extend as much as possible the continuous operation and increase the evaporation pressure at the same time. Furthermore, thanks to a better match between the cooling unit and the water loop achieved using T_B as controlled variable, the strategy S_T leads to a considerable increase in the chiller capacity when the high temperature series are compared.

5.2. Daily characterization of the system

The validated numerical model was also used to simulate the three control logics under variable load and ambient condition on a daily cycle. The results were used to assess how the combined variation of loads and ambient temperature impacted on the control strategies performances.

For this purpose, each control logic was tested on three different 24-hour profiles of the thermal load. The three loads were defined as multiple of the experimental load $\dot{Q}_{load,0}$ (see Fig. 5) as recorded on 31st July 2020. The first profile was assumed equal to the experimental one whereas the other two were obtained by multiplying the first by a factor two ($\dot{Q}_{2xload,0}$) and three ($\dot{Q}_{3xload,0}$), respectively. All the remaining boundary conditions and set-points profiles were kept the same for each run. So, a total of nine 24-hour simulations were performed.

Fig. 6 summarises the overall performances of the control strategies S_0, S_p and S_T with respect to the mean values $\overline{\dot{Q}_{load}}$ of the tested thermal loads profiles (i.e. $\overline{\dot{Q}_{load,0}} = 11.9$ kW, $\overline{\dot{Q}_{2xload,0}} = 23.8$ kW, and $\overline{\dot{Q}_{3xload,0}} = 35.7$ kW). In particular, the pressure ratio $\overline{PR}$ and the evaporation temperature $\overline{T_6}$ are the average of the corresponding quantities, while COP was calculated as the ratio between the total cooling energy and the total compressor energy consumption.

The numerical model demonstrated that considering alternative control strategies can result in significant energy efficiency increases. Especially, S_T resulted in mean COP values that were around +5.8% ($\dot{Q}_{load,0}$), +11.2% ($\dot{Q}_{2xload,0}$), and +11.3% ($\dot{Q}_{3xload,0}$) higher than the COPs obtained with S_0. As also suggested by the steady-state simulations, these increases were more evident for relatively high mean thermal loads values (i.e. $\dot{Q}_{2xload,0}$ and $\dot{Q}_{3xload,0}$ profiles). The benefits are of course related to the higher mean evaporation temperature T_6 values, which result in a more efficient heat exchange at the flooded evaporator and lower compression ratios. In contrast, the control strategy S_p did not yield any remarkable improvement in system performance: small increases of around 0.2% and 1.5% were observed in the COP for $\dot{Q}_{load,0}$ and $\dot{Q}_{3xload,0}$, whereas for the case $\dot{Q}_{2xload,0}$ a decrease of −2.3% was even observed in comparison of S_0, which implies that the average thermodynamic cycle improvement is insufficient to offset the inverter efficiency by a considerable margin.

This can be explained by observing the trends of COP, temperature of the water supplied to the flooded evaporator T_A, chilled water temperature T_B, and compressor rotational speed n_C, in the interval with higher cooling demand of the simulated day (10:00–20:00), as depicted in Fig. 7. Both the strategies S_p and S_T increased the duty cycle of the system when compared to S_0. Nevertheless, the strategy S_p led to lower values of the temperature T_A of the water entering the flooded evaporator, due to poorer coupling between the cooling unit and the water loop. This resulted in lower evaporation temperatures and, consequently, higher pressure ratios, which along with higher values of the compressor rotational speed determined a higher overall energy consumption of the compressor.

6. Conclusions

In this paper, we first presented the dynamic model of an inverter-controlled transcritical CO2 unit that operates in chiller configuration. The numerical model was validated against experimental data and used to investigate steady-state and dynamic performance of the refrigerating system, coupled with a water storage tank, under off-design operating conditions. Three different control strategies were implemented and compared. The first control logic considered the compressor operating at fixed rotational speed, corresponding to a compressor frequency of 50 Hz. In the second control logic the compressor operated at variable speed controlled by the evaporation pressure to resemble the real control strategy. Finally, in the third control logic the compressor frequency was set equal to 30 Hz when the chilled water temperature was below 12 °C, and an additional PID controller intervened, if necessary, to adapt the system capacity to the cooling demand and maintain the water temperature at a maximum value of 12 °C, by varying the compressor frequency between 30 Hz and 60 Hz. Results depicted that the first two logics performed with no significant differences, and, at the same time, the third case study provided the highest energy savings. This proves that the lack of self-awareness about the operating conditions of the refrigerating system hinders the control system in achieving the highest possible performance. The analysis of the results suggests opportunities related to the integration of advanced control systems that could take advantage of considerations about system behaviour in steady-state and of historical operational data to improve the system self-awareness and ability to adapt the control logic to the specific application. Due to the intrinsic characteristics of the considered application, the control performance could be further improved if one uses predictive control approaches (e.g., disturbance predictions). Therefore, following a Co-Design approach, the simulation environment will be deployed in future developments to design and test advanced control strategies to efficiently manage the refrigerating system while guaranteeing thermal loads constraints. In addition, the model will be extended to capture system behaviour in different modes, including heating, heat recovery and production of domestic hot water. Future work will also consider the energy consumptions of gas-cooler fans and water pumps.

Declaration of Competing Interest

The authors declare that they have no known competing financial interests or personal relationships that could have appeared to influence the work reported in this paper.

Data availability

Data will be made available on request.

References

[1] V. Vakiloroaya, B. Samali, A. Fakhar, K. Pishghadam, A review of different strategies for HVAC energy saving, Energy Convers Manag. 77 (2014) 738–754, https://doi.org/10.1016/J.ENCONMAN.2013.10.023.

[2] European Commission, The European Green Deal, (n.d.). https://eur-lex.europa.eu/legal-content/EN/TXT/PDF/?uri=CELEX:52019DC0640&from=IT (accessed January 30, 2022).

[3] M. Rampazzo, M. Lionello, A. Beghi, E. Sisti, L. Cecchinato, A static moving boundary modelling approach for simulation of indirect evaporative free cooling systems, Appl Energy. 250 (2019) 1719–1728, https://doi.org/10.1016/j.apenergy.2019.04.087.

[4] A. Beghi, L. Cecchinato, M. Rampazzo, F. Simmini, Energy efficient control of HVAC systems with ice cold thermal energy storage, J Process Control. 24 (2014) 773–781, https://doi.org/10.1016/J.JPROCONT.2014.01.008.

[5] M.A. Khalil, M.R. Fatmi, How residential energy consumption has changed due to COVID-19 pandemic? An agent-based model, Sustain Cities Soc. 81 (2022), 103832 https://doi.org/10.1016/J.SCS.2022.103832.

[6] J. Rouleau, L. Gosselin, Impacts of the COVID-19 lockdown on energy consumption in a Canadian social housing building, Appl Energy. 287 (2021), 116565, https://doi.org/10.1016/J.APENERGY.2021.116565.

[7] REHVA, REHVA COVID-19 guidance document. 2020., How to Operate and Use Building Services in Order to Prevent the Spread of the Coronavirus Disease (COVID-19) Virus (SARS-CoV-2) in Workplaces. Federation of European Heating, Ventilation and Air Conditioning Associations. (2020).

[8] ASHRAE, Issues and Statements on Relationship Between COVID-19 and HVAC in Buildings. (2020).

[9] W. Zheng, J. Hu, Z. Wang, J. Li, Z. Fu, H. Li, J. Jurasz, S.K. Chou, J. Yan, COVID-19 Impact on Operation and Energy Consumption of Heating, Ventilation and Air-Conditioning (HVAC) Systems, Advances in Applied Energy. 3 (2021), 100040, https://doi.org/10.1016/J.ADAPEN.2021.100040.

[10] M. Guo, P. Xu, T. Xiao, R. He, M. Dai, S.L. Miller, Review and comparison of HVAC operation guidelines in different countries during the COVID-19 pandemic, Build Environ. 187 (2021), 107368, https://doi.org/10.1016/J.BUILDENV.2020.107368.

[11] C.A. Faulkner, J.E. Castellini, W. Zuo, D.M. Lorenzetti, M.D. Sohn, Investigation of HVAC operation strategies for office buildings during COVID-19 pandemic, Build Environ. 207 (2022), 108519, https://doi.org/10.1016/J.BUILDENV.2021.108519.

[12] L. Schibuola, C. Tambani, High energy efficiency ventilation to limit COVID-19 contagion in school environments, Energy Build. 240 (2021), 110882, https://doi.org/10.1016/J.ENBUILD.2021.110882.

[13] M.J. Risbeck, M.Z. Bazant, Z. Jiang, Y.M. Lee, K.H. Drees, J.D. Douglas, Modeling and multiobjective optimization of indoor airborne disease transmission risk and associated energy consumption for building HVAC systems, Energy Build. 253 (2021), 111497, https://doi.org/10.1016/J.ENBUILD.2021.111497.

[14] Z. Jiang, Z. Deng, X. Wang, B. Dong, PANDEMIC: Occupancy driven predictive ventilation control to minimize energy consumption and infection risk, Appl Energy. 334 (2023), 120676, https://doi.org/10.1016/j.apenergy.2023.120676.

[15] M. Garcia-Sanz, Control Co-Design: An engineering game changer, Advanced Control for Applications: Engineering and Industrial Systems. 1 (2019) e18.

[16] M.A. Brdyś, K. Malinowski, Computer Aided Control System Design, WORLD SCIENTIFIC (1994), https://doi.org/10.1142/2020.

[17] A. Varga, Computer-Aided Control Systems Design: Introduction and Historical Overview, Encyclopedia of Systems and Control. (2020) 1–7, https://doi.org/10.1007/978-1-4471-5102-9_138-3.

[18] M. Casini, Chapter 10 - Building automation systems, in: M. Casini (Ed.), Construction 4.0, Woodhead Publishing, 2022: pp. 525–581. 10.1016/B978-0-12-821797-9.00008-8.

[19] A.I. Dounis, C. Caraiscos, Advanced control systems engineering for energy and comfort management in a building environment—A review, Renewable and Sustainable Energy Reviews. 13 (2009) 1246–1261, https://doi.org/10.1016/J.RSER.2008.09.015.
[20] A. Afram, F. Janabi-Sharifi, Theory and applications of HVAC control systems – A review of model predictive control (MPC), Build Environ. 72 (2014) 343–355, https://doi.org/10.1016/J.BUILDENV.2013.11.016.
[21] ASHRAE, 2008 ASHRAE Handbook – HVAC Systems and Equipment (I-P): I-P Edition, American Society of Heating Refrigerating & Air Conditioning Engineers Incorporated, Place of publication not identified. 2008.
[22] ASERCOM, ASERCOM guidelines for the design of multiple compressor racks using frequency inverters, 2017. https://iifiir.org/en/fridoc/asercom-guidelines-for-the-design-of-multiple-compressor-racks-using-4725 (accessed December 6, 2022).
[23] A. Beghi, L. Cecchinato, G.D. Mana, M. Lionello, M. Rampazzo, E. Sisti, Modelling and control of a free cooling system for Data Centers, Energy Procedia. 140 (2017) 447–457, https://doi.org/10.1016/J.EGYPRO.2017.11.156.
[24] ASHRAE, ASHRAE Handbook – Heating, ventilating, and air-conditioning applications, SI edition, ASHRAE, Atlanta, Ga, 2011, p. 2011.
[25] P. Artuso, G. Tosato, A. Rossetti, S. Marinetti, A. Hafner, K. Banasiak, S. Minetto, Dynamic Modelling and Validation of an Air-to-Water Reversible R744 Heat Pump for High Energy Demand Buildings, Energies (Basel). 14 (2021) 8238, https://doi.org/10.3390/en14248238.
[26] B.P. Rasmussen, Dynamic Modeling and Advanced Control of Air Conditioning and Refrigeration Systems, 2005. https://www.ideals.illinois.edu/handle/2142/83841 (accessed January 27, 2022).
[27] G. Tosato, P. Artuso, S. Minetto, A. Rossetti, Y. Allouche, K. Banasiak, Experimental and numerical investigation of a transcritical CO2 air/water reversible heat pump: analysis of domestic hot water production, in: Proceedings of the 14th IIR-Gustav Lorentzen Conference on Natural Refrigerants, IIR, 2020.
[28] G. Schweiger, H. Nilsson, J. Schoeggl, W. Birk, A. Posch, Modeling and simulation of large-scale systems: A systematic comparison of modeling paradigms, Appl Math Comput. 365 (2020), 124713, https://doi.org/10.1016/J.AMC.2019.124713.
[29] P. Artuso, G. Tosato, A. Hafner, A. Rossetti, S. Minetto, S. Marinetti, 02_Data_Site-2.txt, Replication Data for: MultiPACK Project: Field Data of Integrated CO2 Heat Pump Systems for Italian Hotels in the MultiPACK Project. (2021). 10.18710/UNIYBZ/6DR3LK.